Pergamon

Tetrahedron: *Asymmetry* 11 (2000) 37–51

TETRAHEDRON:
ASYMMETRY

The solution conformation of glycosyl inositols related to inositolphosphoglycan (IPG) mediators

M. Martin-Lomas,* P. M. Nieto, N. Khiar, S. García, M. Flores-Mosquera, E. Poirot, J. Angulo and J. L. Muñoz

Grupo de Carbohidratos, Instituto de Investigaciones Químicas, CSIC-UNSE, Américo Vespucio s/n, 41092 Sevilla, Spain

Received 1 December 1999; accepted 15 December 1999

Abstract

The preferred solution conformation of the pseudodisaccharides **7**–**15**, containing the structural motifs that have been proposed for the putative inositolphosphoglycan (IPG) mediators of intracellular signalling processes, have been investigated using NMR spectroscopy and molecular mechanics calculations. The results indicate that the different structural motifs (α and β 1–6 or α and β 1–4 glucosaminyl-D-*myo*-inositol; α and β 1–6 glucosaminyl-D-*chiro*-inositol) adopt various three-dimensional shapes that may modulate their biological properties.

1. Introduction

Several lines of evidence seem to indicate that the binding of a number of growth factors, classical hormones and cytokines to their receptors results in the enzymatic cleavage of uncharacterised glycosyl phosphatidylinositols (GPIs) to give inositolphosphoglycans (IPGs) that modulate the activity of intracellular enzymes and mediate a variety of intracellular events.[1] The scarcity of biologically active material that can be obtained from mammalian tissues has prevented the unequivocal determination of the precise chemical structure of the IPG mediators; however, two main structural groups have been proposed on the basis of chemical composition and biological activity:[2,3] the family of the inhibitors of the c-AMP dependent protein kinase (PKA)[2], which contain *myo*-inositol, non-acetylated glucosamine and phosphate and the family of the activators of pyruvate dehydrogenase phosphatase (PDH phosphatase),[3] which contain *chiro*-inositol, non-acetylated galactosamine and phosphate. Neither the nature of the enzymes involved in GPI cleavage [most likely a phosphatidylinositol specific phospholipase C (PI-PLC) or D (PI-PLD)] nor the mechanism by which this enzyme is regulated are known, and detailed studies of the specific structural requirements involved either in GPI cleavage or IPG activity are lacking.

* Corresponding author.

0957-4166/00/$ - see front matter
PII: S0957-4166(99)00588-1

We are engaged[4–8] in studies directed at establishing the molecular basis of this new intracellular signalling mechanism by synthesising a variety of IPG-like structures, on the basis of the already existing partial structural data on naturally occurring IPGs, and investigating some aspects of their potential biological activity. In order to perform structure–activity studies involving key enzymes in the signalling process possessing well-defined binding site geometries, such as PKA and glycogen synthase phosphatase 2C,[9–13] the three-dimensional structure of these synthetic IPG-like compounds has to be determined. As a continuation of previous studies in which the conformation of a series of substances containing the most commonly encountered glucosaminyl α(1–6)-D-*myo*-inositol structural motif was established, we now report on the solution conformation of a variety of synthetic IPG-like structures that may reasonably be involved in the signalling process.

In previous papers we reported[5] on the solid-state structure of *O*-2-ammonio-2-deoxy-α-D-glucopyranosyl-(1–6)-D-*myo*-inositol-1,2-cyclic phosphate **1** and on the solution conformation of **1**, *O*-2-ammonio-2-deoxy-α-D-glucopyranosyl-(1–6)-D-*myo*-inositol-1-phosphate **2**, and *O*-α-D-mannopyranosyl (1–4)-*O*-2-ammonio-2-deoxy-α-D-glucopyranosyl-(1–6)-D-*myo*-inositol-1,2-cyclic phosphate **3**. Compounds **1** and **2** are expected to be the products generated from a glycosyl phosphatidyl-inositol such as **4** after PI-PLC hydrolysis while compound **3** is expected to be one of the products generated from a glycosyl phosphatidylinositol such as **5** after PI-PLC cleavage. It was concluded that the three-dimensional structures of compounds **1** and **2** may be described by a major conformer that undergoes torsional oscillations around a global minimum in which the charged ammonium and phosphate groups appear close in space, particularly in the case of compound **2**. The ^{31}P and ^{1}H NMR spectra of these compounds were analysed as a function of pH and the data provided relevant information regarding the influence of the ionisation state of the ammonium and phosphate groups on the distinct conformational behaviour of these compounds. Other zwitterionic members of this family of compounds bearing the glucosaminyl α(1–6)-D-*myo*-inositol structural motif such as **3**[5] or the pseudopentasaccharide that constitute the conserved linear structure of the GPI anchors **6**[8] showed a similar conformational behaviour.

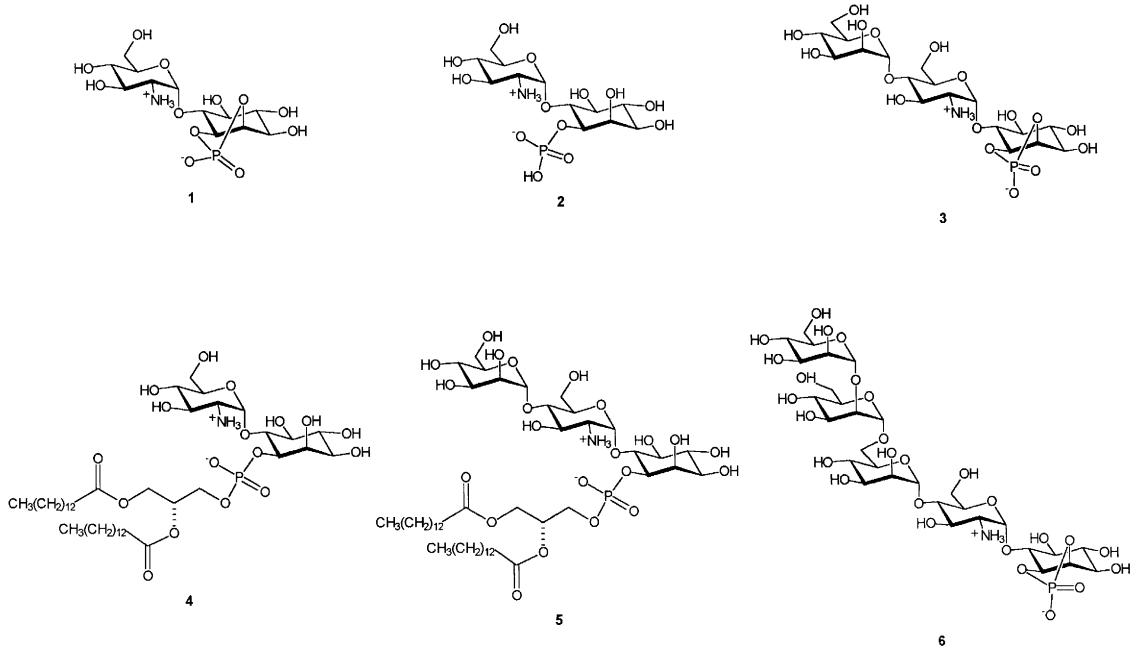

The study of the conformation of these IPG-like structures containing the glucosaminyl α(1–6)-

D-*myo*-inositol structural motif has now been completed with compounds *O*-2-amino-2-deoxy-α-D-glucopyranosyl (1–6)-D-*myo*-inositol **7** and *O*-2-ammonio-2-deoxy-α-D-glucopyranosyl (1–6)-L-*myo*-inositol-1,2-cyclic phosphate **8**. Compound **7** is the product to be expected from **5** after PI-PLD cleavage while compound **8** contains the same basic structural motif as **1** but the L-configuration of the *myo*-inositol moiety (or the α 1–4 glycosidic linkage in the D-series) since this motif has previously been suggested to be involved in the insulin signalling process.[2,14] On the other hand, the solution conformation of the β-configurated compounds *O*-2-ammonio-2-deoxy-β-D-glucopyranosyl (1–6)-D-*myo*-inositol **9** and *O*-2-ammonio-2-deoxy-β-D-glucopyranosyl (1–6)-L-*myo*-inositol-1,2-cyclic phosphate **10** have been investigated as these structural motifs were recently proposed to be present in biologically active substances.[15,16] Finally, the conformational behaviour in solution of the D-*chiro*-inositol-containing compounds, either with the α- or β-configuration, *O*-2-amino-2-deoxy-α-D-glucopyranosyl (1–6)-D-*chiro*-inositol **11**, *O*-2-ammonio-2-deoxy-α-D-glucopyranosyl (1–6)-D-*chiro*-inositol-1,2-cyclic phosphate **12**, *O*-2-ammonio-2-deoxy-α-D-glucopyranosyl (1–6)-D-*chiro*-inositol-1-phosphate **13**, *O*-2-amino-2-deoxy-β-D-glucopyranosyl (1–6)-D-*chiro*-inositol **14** and *O*-2-ammonio-2-deoxy-β-D-glucopyranosyl (1–6)-D-*chiro*-inositol **15** has been investigated.

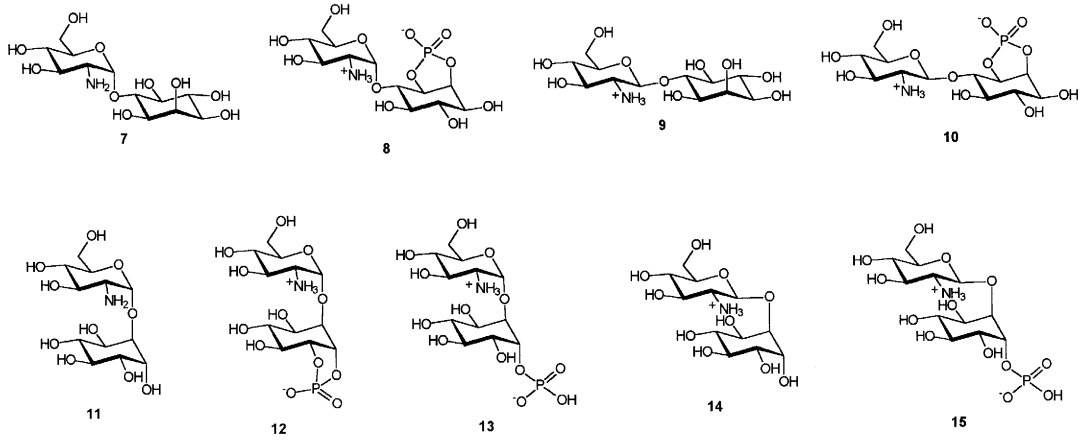

2. Results and discussion

The conformational analysis of compounds **7**–**15** in solution has been carried out by NMR spectroscopy and molecular mechanics calculations.[17] The AMBER* force field,[18] which is parameterised for pyranoses and provides adequate parameters for the phosphate groups, has been used for the calculations. In addition to the glycosidic torsion angles, Φ_H (H1′–C1′–O1–C6) and Ψ_H (C1′–O1–C6–H6), all possible conformations of the phosphate group, those of the hydroxymethyl group, and the clockwise and anticlockwise orientations of the secondary hydroxyl groups have been considered in the calculations. The NMR spectra of all compounds **7**–**15** were assigned using standard 2D techniques (COSY, TOCSY, NOESY and ROESY). NOE and ROE have been measured using 1D selective NOESY, ROESY and TROESY with a DPFGSE selection module using at least six different mixing times (from 600 to 100 ms). Cross relaxation rates (σ_{NOE}, σ_{ROE}, σ_{TROE}) were obtained from these values by extrapolation at zero mixing time,[19] and interprotonic distances were evaluated assuming isolated spin pairs approximation, and using the closest glucosamine distance as known distance. This technique is sensible enough as to allow detecting enhancements of 1%.

2.1. *The glucosamine α 1–6* myo-*inositol structural motif*

The adiabatic surfaces built from the relaxed maps and the corresponding probability distribution maps superimposed on the key NOEs predicted for compounds **7** and **8** are shown in Figs. 1 and 2, respectively. In both cases two local minima are predicted, the lower energy one describing the *syn*-conformation, and the higher energy one corresponding to an *anti*-conformation, as could be expected as a result of the *exo*-anomeric effect. The overall description of the populated conformational space is similar in both cases and in agreement with previous findings for the α(1–6)-linked structures **1** and **2**, although the population distribution maps calculated from the whole set of conformers predict for **7** and **8** a population lower than 1% for the high energy minimum. The *syn*-Ψ minimum is characterised by the H1′–H6 exclusive NOE while the *anti*-Ψ minimum is characterised by the H1′–H5 and H1′–H1 contacts. These three exclusive NOEs are observed for **7** and **8**, which indicate that these two predicted conformers are present in a fast equilibrium (Table 1). For compound **8** the shorter interprotonic experimental distance corresponding to H1′–H6 indicates that, according to the molecular mechanics predictions, the highest populated area lays around the *syn*-minimum. For compound **7**, strong coupling and overlapping between H1′ and H6 prevents the measurement of the individual NOE values and therefore the calculation of the experimental distances. However, a qualitative analysis could be carried out in this case using an HMQC–NOESY where the ^{13}C chemical shift values for C1′ and C6 in the indirect dimension are different enough as to permit the distinction of the individual NOE peaks. Also, in this case the strongest contact corresponded to the H1′–H6 peak.

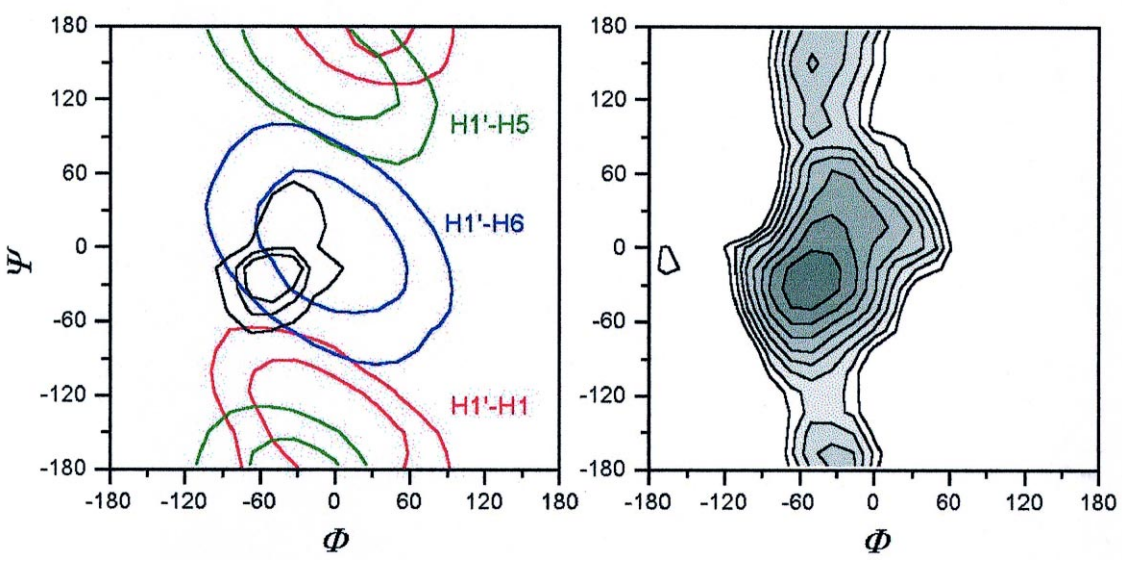

Fig. 1. Relaxed adiabatic energy map (left) calculated for compound **7**, and superimposition of the key NOEs predicted for compound **7** on the conformational probability distribution plot (right). The level contours are given every 5 kJ mol^{-1} for the energy, the interprotonic distances at 2.5 and 3 Å and the probability at 10, 5 and 1%

From the above NMR results it can be concluded that the three-dimensional structures of both **7** and **8** in solution may be described by a major conformer (*syn*-Ψ) in fast equilibrium with a minor conformer (*anti*-Ψ). There is, therefore, a discrepancy between the experimental results and the theoretical predictions that fail to properly evaluate the weight of the *anti*-Ψ minimum in this system. These results are also apparently in contradiction with our previous work[5] that, also using the AMBER force field[20] but with different modifications[21] to include the anomeric and *exo*-anomeric effect, concluded that the three-

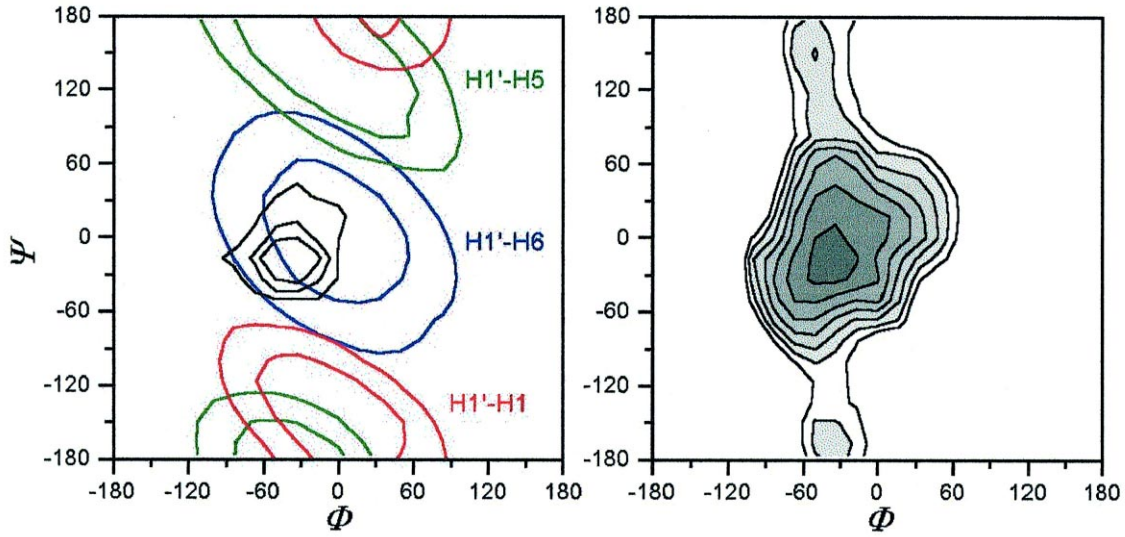

Fig. 2. Relaxed adiabatic energy map (left) calculated for compound **8**, and superimposition of the key NOEs predicted for compound **8** on the conformational probability distribution plot (right). The level contours are given every 5 kJ mol^{-1} for the energy, the interprotonic distances for 2.5 and 3 Å and the probability at 10, 5 and 1%

Table 1
Experimental cross-relaxation rates, σ and experimental and calculated distances in D_2O at 25°C, for **7** and **8**

		NOESY		ROESY		
	Proton Pair	σ s^{-1}	Exp.	σ s^{-1}	Exp.	Calcd.
7	H1'-H2'	0.081		0.093		
	H1'-H6 + H1'-H1	0.112		0.058		
	H1'-H5	0.014	3.41	0.009	3.23	3.72
8	H1'-H2'	0.074		0.078		
	H1'-H5	0.018	3.00	0.076	2.38	4.51
	H1'-H6	0.077	2.35	0.189	2.05	2.28
	H1'-H1	0.011	3.24	0.010	3.35	3.86

dimensional structures of **1** and **2** could be almost exclusively described by a major conformer (*syn*-Ψ); this then being substantiated by NMR as the minor conformer (*anti*-Ψ) also could not be experimentally detected. The experimental observation of the presence of the minor conformer in the cases of **7** and **8**, but not for compounds **1** and **2** could, however, be rationalised taking into account the higher flexibility of the glycosidic linkage of **7**, due to the lack of electrostatic interaction, and the different spatial arrangement of the ammonium and phosphate groups in **8** as compared to **1** and **2**. In the case of the latter compounds the electrostatic interaction should favour the *syn*-Ψ conformation while an opposite effect could be expected for **8** since the calculated geometries predict a favourable interaction in the *anti*-Ψ situation. The NOE ratio between H1′–H2′ and H1′–H5′ for compounds **7** and **8** (H1′–H2′/H1′–H5′, 5.8 for **7** and 4 for **8**) indicates a somehow higher weight of *anti*-Ψ conformer in the case of **8**. A full minimisation carried out on the *syn*-Ψ and *anti*-Ψ lower energy structures taken from the adiabatic energy maps indicates the possibility of opposite stabilising effects (Fig. 3). On one side, the *syn*-Ψ structure presents a hydrogen bond between the hydroxyl group in position 6 of the glucosamine and an oxygen of the inositol phosphate group. On the other side, the **8** *anti*-Ψ conformer could be stabilised by electrostatic

interactions between the charged groups. As a result of this balance, only a small deviation towards the *anti*-minimum with respect to **7** was found.

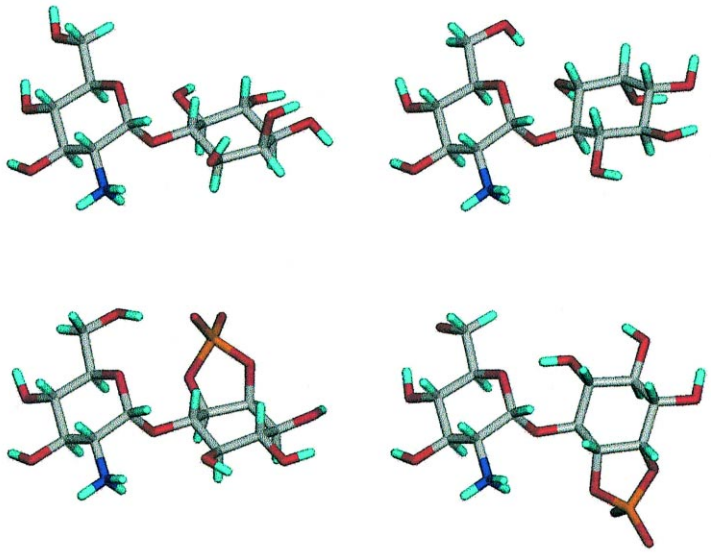

Fig. 3. Minimised structures for **7** (top) and **8** (bottom) in *syn*- (left) and *anti*- (right) conformations

2.2. *The glucosamine β 1–6* myo-*inositol structural motif*

The three-dimensional structures in solution of compounds **9** and **10** have been similarly studied. The corresponding adiabatic surfaces and population distribution maps superimposed on the predicted exclusive NOEs are given in Figs. 4 and 5. As may be expected for a β-glycosidic structure three minima (*syn*-Ψ, *anti*-Ψ and *anti*-Φ) are predicted, the *syn*-Ψ being the energetically favoured conformation. The key NOEs that characterise these minima are H1′–H6′ for the *syn*-Ψ situation (this may also be accompanied by a weak H1′–H1′ contact), H1′–H1′ and H1′–H5′ for the *anti*-Ψ orientation, and H2′–H6 for the *anti*-Φ arrangement. The NOESY spectrum of **9** shows strong H1′–H6′ and weak H1′–H1 peaks. The H1′–H5 contact cannot be directly detected because of overlapping with the intraresidue H1′–H5′ although the intensity of the latter, as compared with H1′–H3′, clearly indicates the existence of an H1–H5 contribution. For compound **10** a strong H1′–H6 and two weak H1′–H1 and H1′–H5 cross peaks are observed. Quantitatively, both compounds can be described as in a fast equilibrium between *syn*-Ψ and the *anti*-Ψ conformers with the highest contribution arising from the *syn*-Ψ situation. A quantitative analysis of the experimental data indicates a slightly higher weight of the *syn* conformation for **10** with respect to **9**. The H1′–H1 experimental distance for **9** (Table 2) is shorter, and the σ_{NOE} ratio between exclusive NOEs of the *syn* and *anti* minima (H1′–H6/ H1′–H1 5.8 for **9** and 6.2 for **4**) is bigger for **10**. The structural reason for this difference could be an electrostatic interaction only possible in the *syn* conformation favourable in **10** (Fig. 6).

2.3. *The glucosamine α 1–6* chiro-*inositol structural motif*

For the α-linked D-*chiro*-inositol compounds **11**, **12** and **13** the adiabatic energy maps and conformational probability distribution plots predict a single *syn*-Ψ minimum (Figs. 7–9). The detailed inspection of probability distribution maps shows a similar overall shape of the populated areas with the higher

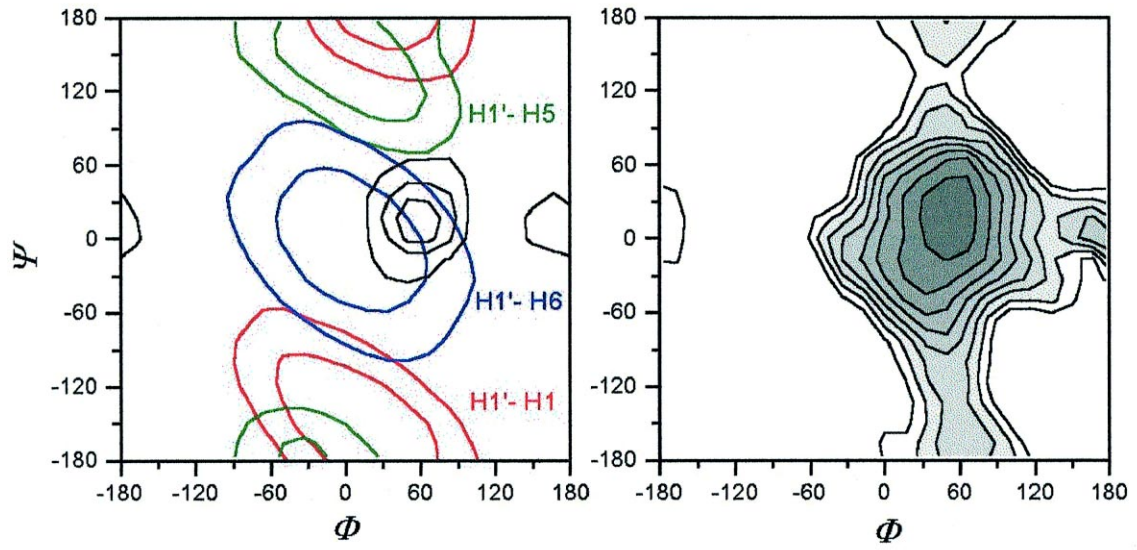

Fig. 4. Relaxed adiabatic energy map (left) calculated for compound **9**, and superimposition of the key NOEs predicted for compound **9** on the conformational probability distribution plot (right). The level contours are given every 5 kJ mol^{-1} for the energy, the interprotonic distances for 2.5 and 3 Å and the probability at 10, 5 and 1%

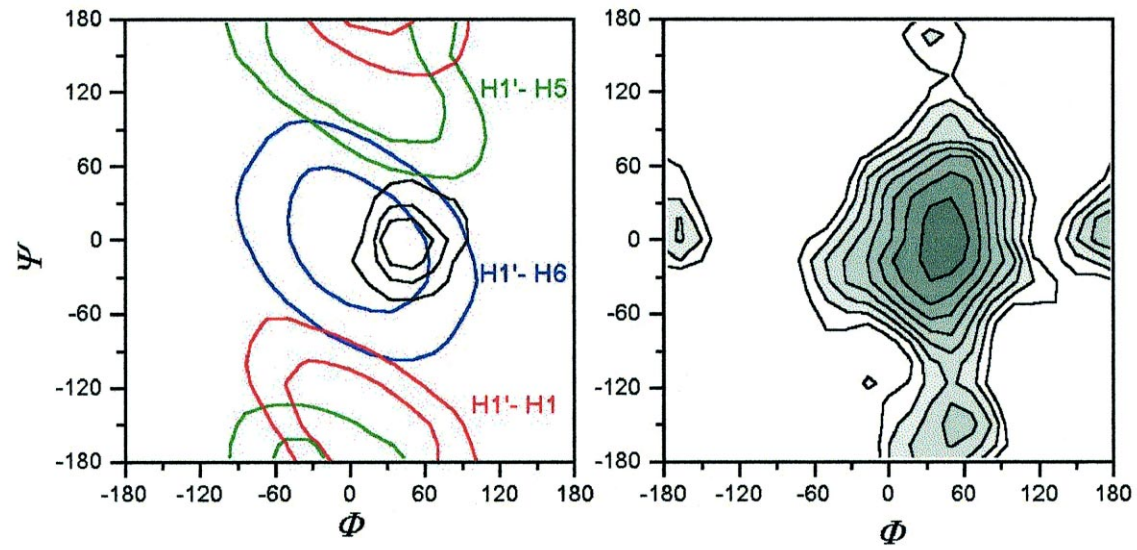

Fig. 5. Relaxed adiabatic energy map (left) calculated for compound **10**, and superimposition of the key NOEs predicted for compound **10** on the conformational probability distribution plot (right). The level contours are given every 5 kJ mol^{-1} for the energy, the interprotonic distances for 2.5 and 3 Å and the probability at 10, 5 and 1%

probability points slightly displaced from one compound to another. For compound **11**, the global minimum resides at A1 Φ −27.0, Ψ 41.8, while for compound **13** the predicted values are Φ −42.4, Ψ 4.7. For compound **12**, a combination of both situations exists with two stable points at Φ −27.2, Ψ 40.2 and Φ 48.3, Ψ 22.9. Thus, according to molecular mechanics calculations a global *syn*-Ψ minimum that can be split into two local subminima (A1 around Φ 30, Ψ 30 and A2 around Φ −40, Ψ 10) are predicted.

Table 2
Experimental cross-relaxation rates, σ and experimental and calculated distances in D_2O at 25°C, for **9** and **10**

		NOESY		ROESY		
	Proton Pair	σ s^{-1}	Exp.	σ s^{-1}	Exp.	Calcd.
9	H1'-H2'	0.018		0.019		
	H1'-H3'	0.063		0.190		
	H1'-H5' + H1'-H5	0.104		0.170		
	H1'-H6	0.128	2.21	0.261	2.35	2.30
	H1'-H1	0.022	2.97	0.047	3.13	4.49
10	H1'-H2'	0.005		0.027		
	H1'-H3'	0.051		0.130		
	H1'-H5'	0.108		0.256		
	H1'-H6	0.103	2.41	0.257	2.39	2.28
	H1'-H1	0.015	3.33	0.024	3.56	4.04
	H1'-H5	0.017	3.27	0.027	3.49	4.53

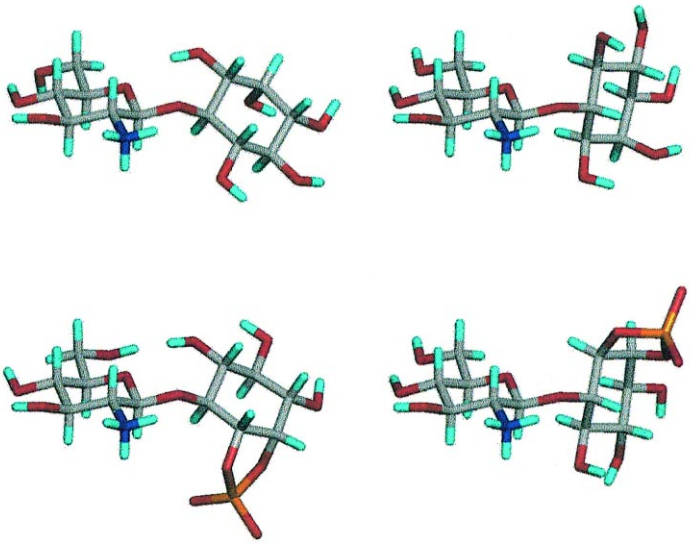

Fig. 6. Minimised structures for **9** (top) and **10** (bottom) in *syn*- (left) and *anti*- (right) conformations

The key contacts that characterise this global minimum are H1′–H6 and H1′–H1 that in this case intersects the highly populated area of the conformational space. The unpredicted *anti*-Ψ minimum would be characterised by the observation of the H1′–H2 and/or H4 contact. The NOESY spectra of **11**, **12** and **13** show strong H1′–H6 and weak H1′–H1 peaks. A small H1′–H5 peak at long mixing times is observed in the case of **11**. Since this contact is not predicted it may be considered artifactual arising either from spin diffusion or through strong scalar coupling. The experimental distances obtained from σ_{NOE} (Table 3) are in good agreement with the predicted values although the H1′–H1 distance is systematically underestimated. When the experimental distances are compared with the r^{-6} average along the molecular dynamics trajectories this agreement is even better and the H1′–H1 are correctly predicted (Table 3). This better fit may indicate the existence of a certain degree of freedom within the populated region and reflects the existence of oscillations around the global minimum.

A further analysis of the experimental results can give more precise information about the conformational properties of this motif. As the intersection of the sort distance regions of H1′–H6 and H1′–H1 contacts is centred on the A2 subminimum, while A1 is out of the H1′–H1 sort contact area, an increase of

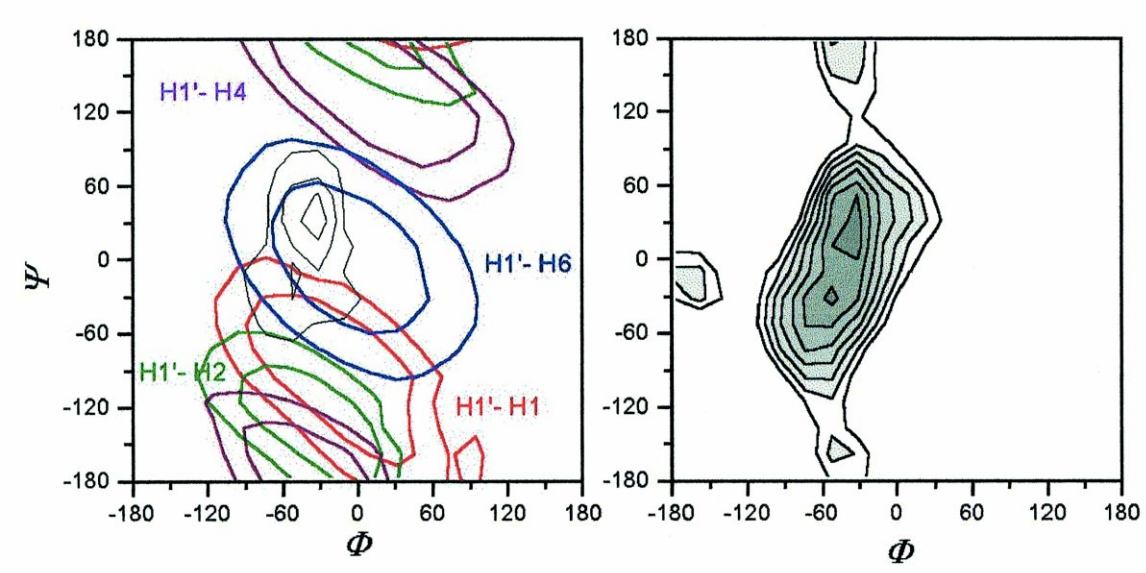

Fig. 7. Relaxed adiabatic energy map (left) calculated for compound **11**, and superimposition of the key NOEs predicted for compound **11** on the conformational probability distribution plot (right). The level contours are given every 5 kJ mol^{-1} for the energy, the interprotonic distances for 2.5 and 3 Å and the probability at 10, 5 and 1%

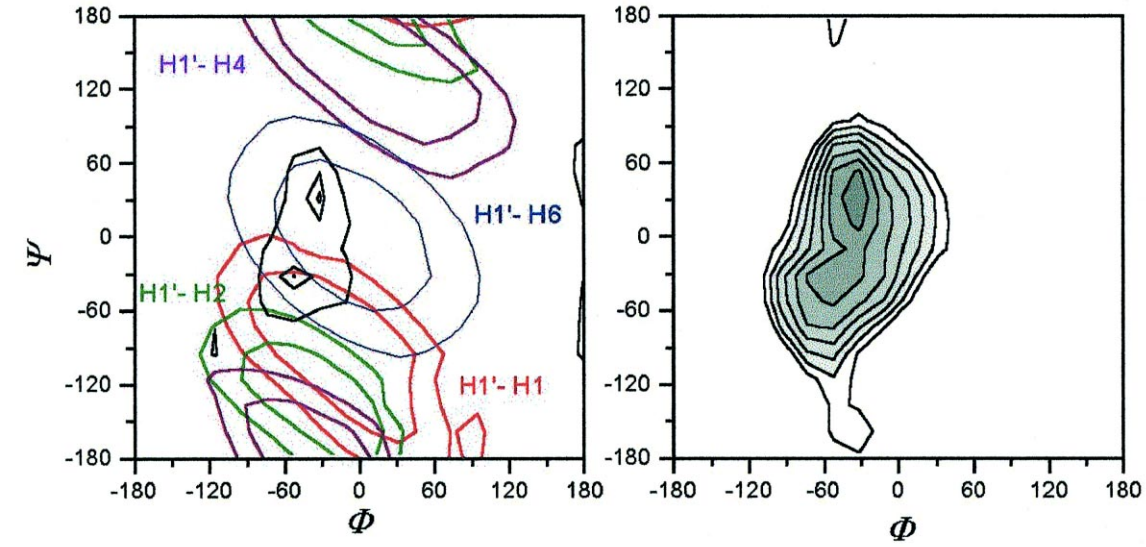

Fig. 8. Relaxed adiabatic energy map (left) calculated for compound **12**, and superimposition of the key NOEs predicted for compound **12** on the conformational probability distribution plot (right). The level contours are given every 5 kJ mol^{-1} for the energy, the interprotonic distances for 2.5 and 3 Å and the probability at 10, 5 and 1%

the H1′–H1 distance be expected as the subminimum A2 predominates over A1. The σ_{NOE} ratios between H1′–H6, H1′–H2 and H1′–H1 agree with the population maps predicted by molecular mechanics. Thus, **11**, which has the higher weight for the local minimum A1, has the higher ratio H1′–H1/H1′–H2 (1.2), the more populated subminimum A2 derivative **13** has the lower one (0.9), while **12** exhibits an intermediate value (1.1). Other NOE peaks detected also correspond with this description; in this sense H5′–H4

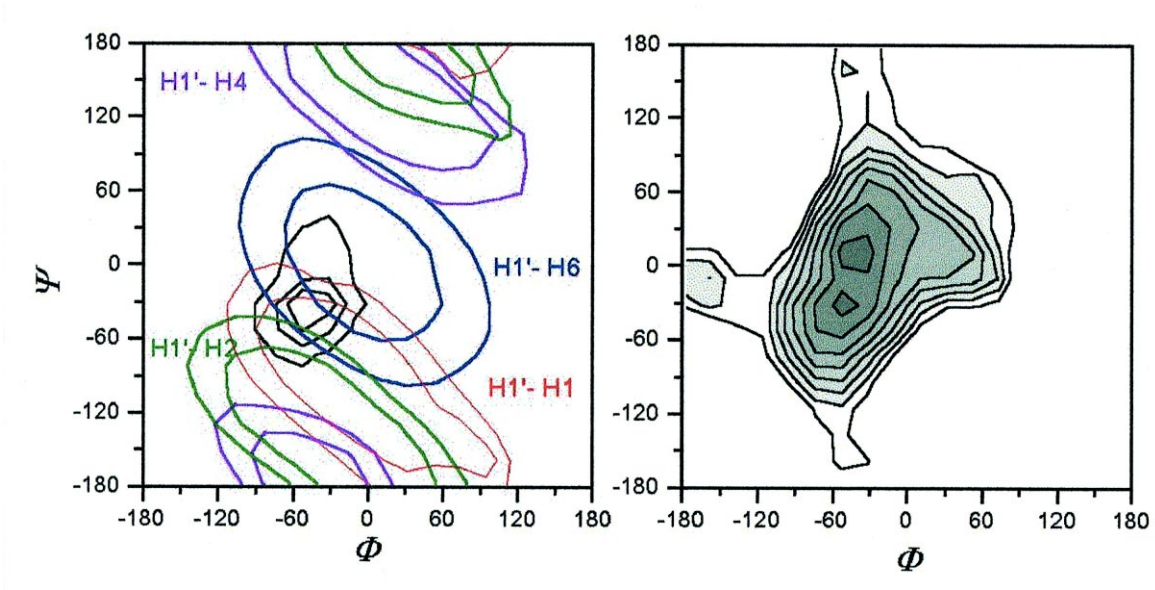

Fig. 9. Relaxed adiabatic energy map (left) calculated for compound **13**, and superimposition of the key NOEs predicted for compound **13** on the conformational probability distribution plot (right). The level contours are given every 5 kJ mol^{-1} for the energy, the interprotonic distances for 2.5 and 3 Å and the probability at 10, 5 and 1%

Table 3
Experimental cross-relaxation rates, σ_{NOE} and experimental and calculated distances in D_2O at 25°C, for **11**, **12** and **13**

					$< r^{-6} >$	
	Proton Pair	σ s^{-1}	Exp.	Calcd.	Exp.	Calcd.
11	H1'-H2'	0.094				
	H1'-H6	0.100	2.37	2.25	2.34	2.4
	H1'-H1	0.081	2.46	4.06	2.42	2.6
12	H1'-H2'	0.123				
	H1'-H6	0.138	2.35	2.25	2.33	2.39
	H1'-H1	0.111	2.44	3.97	2.41	2.52
12	H1'-H2'	0.090				
	H1'-H6	0.104	2.33	2.21	2.31	2.7
	H1'-H1	0.095	2.37	3.19	2.35	2.32

and H5′–H6 could be considered exclusive NOEs of the A1 and A2 subminima, respectively. While compound **11** has a medium NOESY cross peak between H5′ and H4 but not with H6 which are close in an A2 situation, **12** and **13** show the contact H5′–H6 but not the H5′–H4.

This distinct behaviour caused by the presence of the phosphate group in the *chiro*-inositol residue should reflect a different pattern of interactions. Minimisation of the low energy rotamers obtained from the energy maps converges exclusively on minima type A1 for **11**, and on type A2 for **13**, while **12** yields both types (Fig. 10). The A1-type minimised structures show an intra-residue network of hydrogen bonds (4-HO-Ins to 6-O-Glc; 5-HO-Ins to 6-O-Glc; 5-HO-Ins to 5-O-Glc) which interestingly is not possible in type A2 conformations. The electrostatic contribution for the interactions between the ammonium and phosphate groups indicates a stabilisation in the A2 type structures for the phosphorylated derivatives which is bigger in **13** than in **12** (12 and 9 kJ mol^{-1}, respectively). Therefore, two opposite favourable effects operate and their balance directs the conformation towards A1 or A2 subminima. In the case of **11** the hydrogen bond network is the only possible effect, causing the A1 conformer to predominate; the

stronger electrostatic interaction allows derivative **13** to compensate for the loss of this network showing an A2 conformation, but not for **12** which has an intermediate situation.

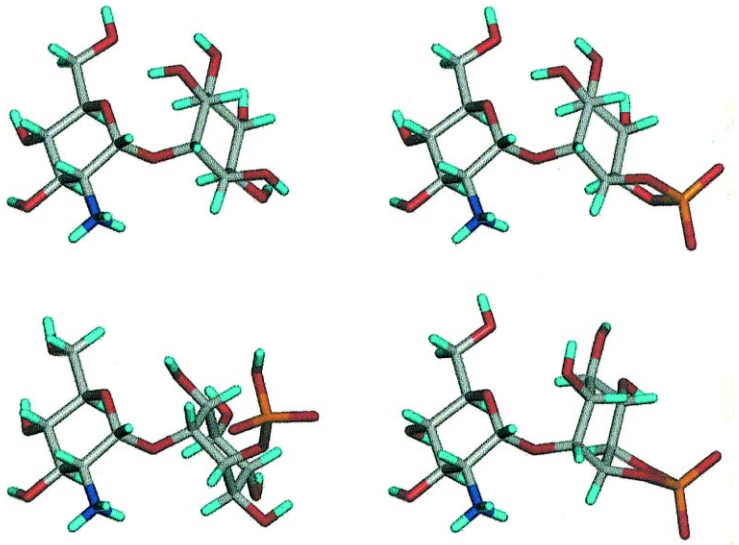

Fig. 10. Minimised structures for the glucosamine α 1–6 *chiro*-inositol motif, subminima A1 (top) for compounds **11** (left) and **12** (right) and subminima A2 (bottom) for compounds **13** (left) and **12** (right)

2.4. The glucosamine β 1–6 chiro-*inositol structural motif*

The energy surfaces and global probability maps for the β-*chiro*-inositol derivatives **14** and **15** given in Figs. 11 and 12 show a single *syn*-Ψ minimum at Φ 56±5, Ψ 17. This prediction is in agreement with the *exo*-anomeric effect in a β disposition. Two NOEs, H1′–H6 and H1′–H1, describe this situation, while an unpredicted *anti*-Ψ conformation would be detected by its key H1′–H2 and H1′–H4 short contacts. Experimentally, only H1′–H6 and H1′–H1 interglycosidic contacts, the latter with smaller intensity, are detected, and no peaks are found for H1′–H2 or H1′–H4, even at large mixing times. Thus, the experimental results are consistent with the predictions, and **14** and **15** are in a *syn*-Ψ disposition and do not show any appreciable contribution from *anti*-Ψ. Experimentally significant distances can be estimated for **15**, and are in good agreement with those calculated by the r^{-6} average along a molecular dynamic trajectory which describes the fluctuation along the minimum (Table 4). Unfortunately, data from the non-phosphorylated compound **13** cannot be quantified due to a severe overlapping of H3′ and H5′ peaks. This compound also shows a spurious cross peak for H1′–H4′ that arises from the H3′–H4′ strongly coupled system. In order to compare the experimental data for the *chiro*-alpha compounds the H1′–H6, H1′–H1 σ_{NOE} ratio was calculated suggesting a very close solution structure for both products: **14** (5.3), **15** (5.3).

The minimum energy structures were calculated over all the possible side group orientations (Fig. 13), and a slight displacement on the torsional angle in the global minimum (**14** Φ 52°, Ψ −17°; **15** Φ 62°, Ψ −17°) was found. A hydrogen bond between the phosphate proton and the pyranose ring oxygen, O-5 Glu, is detected in **15**, which is shorter when the Ψ angle is 62°. This inter-residue interaction can explain the lower dispersion on the Ψ torsional angle average found in the molecular dynamic trajectories (7±31 for **14** and −5±23 for **15**), the narrower *syn*-Ψ minimum for **15**, as well as the values of the Ψ angle.

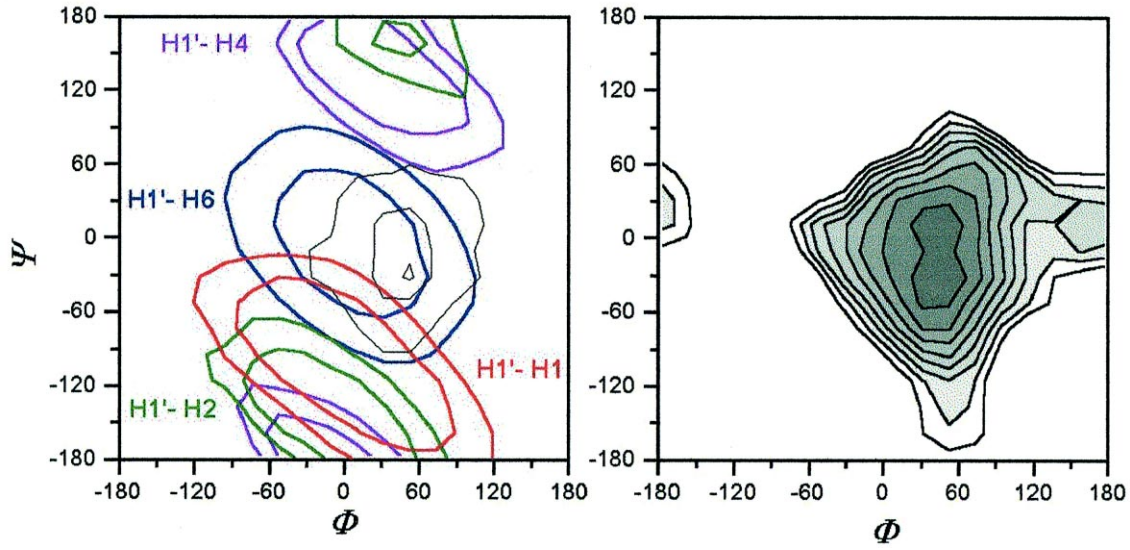

Fig. 11. Relaxed adiabatic energy map (left) calculated for compound **14**, and superimposition of the key NOEs predicted for compound **14** on the conformational probability distribution plot (right). The level contours are given every 5 kJ mol^{-1} for the energy, the interprotonic distances for 2.5 and 3 Å and the probability at 10, 5 and 1%

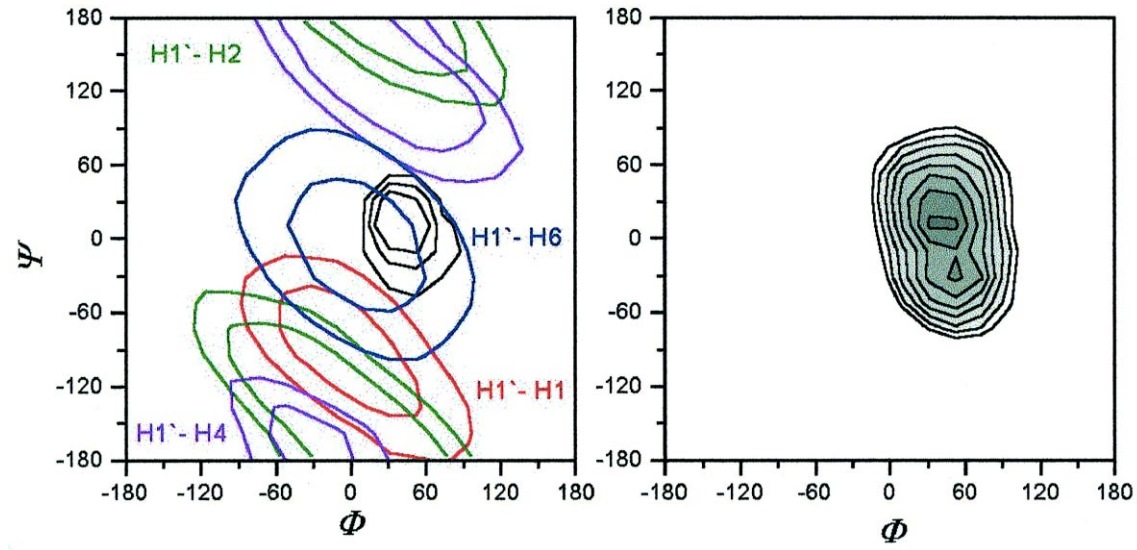

Fig. 12. Relaxed adiabatic energy map (left) calculated for compound **15**, and superimposition of the key NOEs predicted for compound **15** on the conformational probability distribution plot (right). The level contours are given every 5 kJ mol^{-1} for the energy, the interprotonic distances for 2.5 and 3 Å and the probability at 10, 5 and 1%

3. Conclusion

The comparison of the solution structures of GPI-like compounds **7**–**15** allows some general conformational characteristics to be deduced. The *myo*-inositol derivatives **7**–**10** exhibit a marked flexibility not observed in their *chiro*-inositol counterparts, as the latter can be described as a single *syn* conformation. The three-dimensional arrangement of the phosphate moiety with respect to the ammonium group is

Table 4
Experimental cross-relaxation rates, σ_{NOE} and experimental and calculated distances in D_2O at 25°C, for **14** and **15**

	Proton Pair	σ s^{-1}	$< r^{-6} >$ Exp.	Calcd	Exp.	Calcd.
14	H1'-H3' + H1'-H5'	0.117				
	H1'-H4'	0.060				
	H1'-H6	0.156		2.30		2.30
	H1'-H1	0.029		3.77		3.43
15	H1'-H2'	0.023				
	H1'-H3'	0.121				
	H1'-H5'	0.134				
	H1'-H6	0.121	2.49	2.36	2.46	2.28
	H1'-H1	0.023	3.29	3.87	3.24	3.47

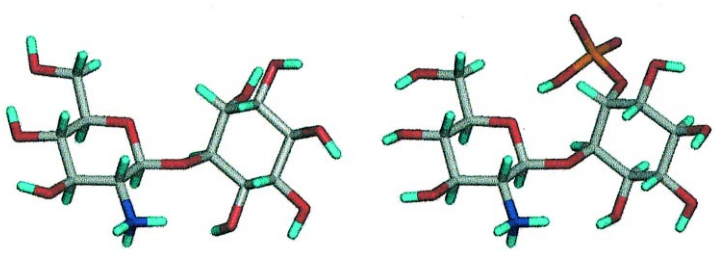

Fig. 13. Minimum energy structures for compounds **14** (left) and **15** (right)

able to modulate the overall conformational preferences given by the glycosidic linkage stereochemistry. In this sense, the observed changes in the *syn*- and *anti*-minima's relative populations found in **8** and **10** as compared with **7** and **9**, where the populations of the phosphorylated compounds' minima shift depending on the anomer (towards *anti* in the case of the α-isomer and to *syn* for the β), should be noted. Similar effects are found in molecules containing the α 1–6 *chiro*-inositol motif. In this case the geometry of the global minimum depends on the substituents on the cyclitol moiety, which influence the relative orientations of the aminosugar and the inositol ring.

From the point of view of the study of the molecular basis of the IPG signalling mechanism, the studied structures provide a wide range of different geometries. In this structural library the glucosamine–cyclitol moiety could also be regarded as a scaffold where the stereochemistry of the linkage of the two rings leads to a broad variety of ammonium–phosphate distributions providing an adequate ensemble for further structure–activity relationship studies.

4. Experimental

Compounds **7**–**15** were synthesised following the methodology described in the literature.[4–8] A detailed report of this synthesis will be published elsewhere.

4.1. NMR measurements

NMR experiments were recorded on a DRX-500 Bruker spectrometer at 25°C. DQF-COSY, TOCSY, HSQC and HMQC experiments used for the full assignment were recorded using the standard *z*-pulsed field gradient enhanced pulse sequences versions when possible. NOESY experiments were recorded

using mixing times from 100 to 600 ms. Selective 1D-NOESY and 1D-TOCSY experiments were recorded using the DPFGSE (double pulsed field gradient spin echo) technique.[22] Due to severe overlapping ^{1}H–^{1}H and ^{31}P–^{1}H coupling constants have been extracted from the dqf-COSY by deconvolution of the 2D antiphase peaks.

4.2. Molecular modelling and molecular dynamics

Gycosidic torsion angles are defined as Φ H-1–C-1–O-1–C–X and Ψ C-1–O-1–C–X–H–X. All the calculations were performed using AMBER*[18] force field parameterised for pyranose oligosaccharides. Solvent effects were included using the GB/SA continuum model for water or ε=80.

Relaxed adiabatic map starting structures were constructed considering all three hydroxymethyl rotamers: *gg*, *gt*, *tg*, clockwise or anticlockwise orientation of the secondary hydroxyl groups, and when necessary the possible combinations of the three possible staggered conformers for the phosphate group were also considered. Then the rigid residue maps were generated for every initial by using a grid step of 20° and every point was optimised. All minimisations were run using up to 9999 Polak–Ribiere conjugate gradient iterations until convergence criterion (rmsd derivatives lower than 0.001 kJ/A mol) was achieved.

Molecular dynamics simulation were run for 2.0 ns with an integration step of 1.5 fs, at a constant temperature of 300 K with a thermal bath coupling constant of 2.5 ps, using SHAKE for hydrogen atoms and saving structures each picosecond with GB/SA solvation model.

4.3. Probability calculations

From the relaxed energy maps, the probability distribution was calculated for each Φ/Ψ point. Assuming that the entropy difference among the different conformers is negligible, the probability *P* of a given Φ/Ψ point is:[23] $P_{\Phi/\Psi}=\sum_i[\exp(-E_i/RT)]/\sum_i\sum_{\Phi/\Psi}[\exp(-E_{i\Phi/\Psi}/RT)]$. This relationship can be used in a simple way to transform energy maps into probability maps.

4.4. Distance calculations

The interproton average distances were estimated from the MD simulations, considering that the interproton distance for every saved frame was calculated according to: $\langle r^{-6}\rangle_{kl}=\sum(1/n)*r^{-6}_{kl(\Phi\Psi)}$, where *n* represents the total number of frames.

Acknowledgements

We thank the Spanish DGES (grant PB96 0820) and The Rademacher Group Ltd for financial support. E.P. and J.A. thank the EU (TMR Programme, CARENET-2) and Fundación Ramón Areces, respectively, for fellowships.

References

1. For recent reviews, see: Jones, D. R.; Varela-Nieto, I.; *Int. J. Biochem. Cell Biol*. **1998**, *30*, 316–326; Stralfors, P.; *Bioessays* **1997**, *19*, 327–335; Field, M. C. *Glycobiology* **1997**, *7*, 161–168; Varela-Nieto, I.; León, Y.; Caro, H. N. *Comp. Biochem. Physiol*. **1999**, *115B*, 223–241.
2. Mato, J. M.; Kelly, K.; Abler, A.; Jarrett, L.; Corkey, B. E.; Cashell, B. E.; Zopl, D. *Biochem. Biophys. Res. Commun*. **1987**, *146*, 764–770.

3. Larner, J.; Huang, L. C.; Schwartz, C. F. W.; Oswal, A. S.; Shen, T. Y.; Kinter, M.; Tang, G.; Zeller, K. *Biochem. Biophys. Res. Commun*. **1988**, *151*, 1416–1426.
4. Khiar, N.; Martin-Lomas, M. In *Carbohydrate Mimics. Concepts and Methods*; Chapleur, Y., Ed.; Wiley-VCH: New York, 1998; pp. 443–462, and references cited therein.
5. Dietrich, H.; Espinosa, J. F.; Chiara, J. L.; Jiménez-Barbero, J.; León, Y.; Varela-Nieto, I.; Mato, J. M.; Cano, F. H.; Foces-Foces, C.; Martin-Lomas, M. *Chem. Eur. J*. **1999**, *5*, 320–336, and references cited therein.
6. Martin-Lomas, M.; Flores-Mosquera, M.; Chiara, J. L. *Eur. J. Org. Chem*., in press.
7. Martin-Lomas, M.; Flores-Mosquera, M.; Khiar, N. *Eur. J. Org. Chem*., in press.
8. Martin-Lomas, M.; Khiar, N.; García, S.; Koessler, J. L.; Rademacher, T. W. *Chem. Eur. J.*, submitted.
9. Taylor, S. S.; Buechler, J. A.; Yonemoto, W. *Ann. Rev. Biochem*. **1990**, *59*, 971–1005.
10. Tamura, S.; Lynch, K. R.; Larner, J.; Fox, J.; Yasui, A.; Kikuchi, K.; Suzuki, Y.; Tsuiki, S. *Proc. Natl. Acad. Sci. USA* **1989**, *86*, 1796–1800.
11. Hünenberger, P. H.; Helms, V.; Narayana, N.; Taylor, S. S.; McCammon, J. A. *Biochemistry* **1999**, *38*, 2358–2366.
12. Narayana, N.; Diller, T. C.; Koide, K.; Bunnage, M. E.; Nicolau, K. C.; Brunton, L. J.; Xuong, N.-H.; Eyck, L. F. T.; Taylor, S. S. *Biochemistry*. **1999**, *38*, 2377–2386.
13. Das, A. K.; Helps, N. R.; Cohen, N. R.; Bardford, D. *EMBO J.* **1996**, *15*, 6798–6809.
14. Mato, J. M., personal communication.
15. Müller, G.; Wied, S.; Piossek, C.; Bauer, A.; Frick, W. *Mol. Med*. **1998**, *4*, 299–323.
16. Frick, W.; Bauer, A.; Bauer, J.; Wied, S.; Müller, G. *Biochemistry* **1998**, *37*, 1421–1436.
17. Woods, R. J. In *Reviews in Computational Chemistry*; Lipkowitz, K. B.; Boyd, D. B., Eds; VCH Publishers: New York, 1996, 129–165.
18. Senderowitz, H.; Still, C. *J. Org. Chem.* **1997**, *62*, 1427–1438.
19. Poppe, L.; Van Halbek, H. *J. Am. Chem. Soc*. **1992**, *114*, 1092–1094.
20. Weiner, S. J.; Kollman, P. A.; Case, D. A.; Singh, U. C.; Ghio, C. *J. Am. Chem. Soc*. **1984**, *106*, 765–784.
21. Homans, S. W. *Biochemistry* **1990**, *29*, 9110–9118.
22. Stott, K.; Keeler, J.; Van, Q. N.; Shaka, A. J. *J. Magn. Reson.* **1997**, *125*, 302–324.
23. Cumming, D. A.; Carver, J. P. *Biochemistry* **1995**, *26*, 6664–6676.